Research Square

Preprints are preliminary reports that have not undergone peer review.
They should not be considered conclusive, used to inform clinical practice,
or referenced by the media as validated information.

Development and Optimization of Parameter Recommendation Model for Automotive Resistance Spot Welding

Yu-Jun Xia

xyjdbgt6509@sjtu.edu.cn

Shanghai Jiao Tong University School of Mechanical Engineering https://orcid.org/0000-0001-6729-8022

YunFan Zhou

Shanghai Jiao Tong University School of Mechanical Engineering

YouRong Zhang

Shanghai Jiao Tong University School of Mechanical Engineering

JianNan Zhang

NIO

YongQuan Jia

NIO

YongBing Li

Shanghai Jiao Tong University School of Mechanical Engineering

Research Article

Keywords: Resistance spot welding, Parameter recommendation, Ensemble learning, Physical constraints, Automotive assembly

Posted Date: September 28th, 2026

DOI: https://doi.org/10.21203/rs.3.rs-10909302/v1

License: This work is licensed under a Creative Commons Attribution 4.0 International License.
Read Full License

Development and Optimization of Parameter Recommendation Model for Automotive Resistance Spot Welding

Yu-Jun Xia[1,*], YunFan Zhou[1], YouRong Zhang[1], JianNan Zhang[2], YongQuan Jia[2], YongBing Li[1,**]

1. Shanghai Key Laboratory of Digital Manufacture for Thin-walled Structures, State Key Laboratory of Mechanical System and Vibration, Shanghai Jiao Tong University, Shanghai, 200240, P.R. China

2. Manufacturing Engineering Integration Department, NIO, Shanghai, 201800, P.R.China

* Corresponding author: E-mail address: xyjdbgt6509@sjtu.edu.cn; Tel.: 86-21-34206305

** Co-Corresponding authors

Abstract

The efficiency and reliability of welding parameter design directly affect weld quality, process stability, and manufacturing responsiveness in automotive manufacturing. Traditional parameter design, heavily reliant on empirical trials and extensive testing, is time-consuming and ill-suited for the growing variety of sheet-stack combinations in modern vehicles. This study proposes an intelligent agent model for parameter generation in Resistance spot welding (RSW). A heterogeneous ensemble learning model to map sheet attributes and target nugget size to welding parameters is established as the base model. On this basis, a novel physics-informed constraint—the heating intensity—which characterizes the heat input path is introduced to address the limitation of purely data-driven base model, particularly its lack of uniqueness and poor generalization. This variable is incorporated into the training process via a multi-loss optimization scheme that simultaneously minimizes parameter prediction error and heating intensity deviation. Results demonstrate that the proposed framework significantly improves prediction accuracy under both same-vehicle and cross-vehicle conditions. Results showed that the heating intensity constraint effectively compresses the solution space, ensuring the uniqueness and physical consistency of generated parameters. By adjusting the heating intensity, the model can controllably generate strong-regime and weak-regime parameter combinations, thereby enhancing the engineering applicability and interpretability of the ensemble learning approach for automotive RSW parameter design. This study paves the way for intelligent management of the entire design and manufacturing of RSW process.

Keywords: Resistance spot welding; Parameter recommendation; Ensemble learning; Physical constraints; Automotive assembly

1. Introduction

In modern manufacturing, particularly in the automotive industry, process-parameter design is a cornerstone of product quality, production efficiency, and manufacturing responsiveness. Recent studies on advanced joining processes have demonstrated that key process variables and thermo-mechanical

conditions can strongly affect interfacial evolution and joint performance [1, 2]. Related studies have further shown that residual-stress states and engineered surface/interface conditions can substantially influence the fracture and bonding performance of joined structures [3, 4]. For resistance spot welding (RSW), which is extensively used in body-in-white assembly, parameter selection directly determines joint quality and manufacturing consistency [5, 6]. As the automotive industry advances lightweighting and adopts more advanced high-strength steels, the complexity of material combinations has increased markedly. Each sheet-stack combination requires a suitable set of welding parameters (current, time, and force) to produce a robust weld. Consequently, rapid and reliable parameter determination has become a critical challenge affecting development cycles and production responsiveness [7, 8]. Traditional approaches to RSW parameter design, such as weldability-lobe testing and design of experiments (DoE), are well established but inherently time-consuming and costly. Response surface methodology and the Taguchi method have been used effectively for localized optimization [9, 10], but their applicability is often limited to specific material systems and predefined experimental spaces, resulting in poor generalizability to new combinations [11, 12]. Although advanced multiphysics finite-element models provide detailed mechanistic insight and can support synthetic-data generation, their computational cost and modeling complexity limit their use for rapid, routine parameter generation [13].

To address the need for rapid and adaptive parameter design, data-driven methods have gained traction. Neural networks, support vector machines, and ensemble learning models have demonstrated the ability to model the complex nonlinear relationships between inputs and weld quality [14-16]. Recent studies have extended data-driven approaches from conventional weld-quality prediction toward process monitoring, parameter optimization, and knowledge-enhanced modeling. Early investigations showed that welding-process signals contain valuable information about nugget formation and weld performance. Cho and Rhee developed a neural-network pattern-recognition method using dynamic-resistance signals for weld-quality estimation [17]. El Ouafi et al. further applied artificial neural networks to RSW quality assessment [18], while Yu used logistic regression with welding-power signals to extract process-related information for weld evaluation [19]. Xia et al. quantitatively interpreted the evolution of dynamic resistance and showed that its trend is governed primarily by the average sheet temperature and electrode/sheet contact diameter rather than by nugget growth alone [20].

With advances in machine-learning algorithms and sensing technologies, more sophisticated models have been investigated for RSW quality prediction and online monitoring. Xing et al. developed a random-forest quality-assessment method using features extracted from dynamic-resistance signals [21]. Zamanzad Gavidel et al. compared several machine-learning algorithms for nugget-width prediction and showed the value of nonlinear models for relating welding parameters to nugget characteristics [22]. Zhou et al. incorporated domain knowledge into models trained on industrial RSW data [23], and Dai et al. developed a deep-learning framework for online inspection using large-scale automotive-production

data [24]. Comparative work has further emphasized that predictive performance should be interpreted together with the data distribution, feature representation, and physical plausibility of model behavior [25]. Beyond weld quality prediction, recent studies have attempted to extend machine learning methods toward welding parameter optimization and intelligent process design. He et al. combined machine learning-based quality prediction with optimization algorithms to achieve simultaneous weld quality evaluation and parameter optimization, demonstrating the potential of automated welding schedule determination [26]. Deng et al. proposed a Bayes-XGBoost and particle swarm optimization framework, in which a nonlinear prediction model was coupled with optimization algorithms to search for welding parameters corresponding to desired quality requirements [27]. Bayir et al. further investigated machine-learning-assisted parameter tuning strategies for automotive resistance spot welding, indicating the feasibility of applying data-driven methods for process adjustment and defect reduction [28].

Meanwhile, improving model adaptability across material combinations and manufacturing conditions has become an important research direction. York et al. introduced a transfer-learning-enhanced Transformer for virtual process sensing, showing that welding metadata and transfer strategies can improve generalization across material stack-ups and welding conditions [29]. Recent studies have further incorporated welding-process physics into data-driven models to improve model robustness and out-of-distribution generalization [30, 31]. Meanwhile, multi-physical simulations have been developed to provide reliable synthetic data and facilitate model generalization across different sheet stack-ups [32].

Despite these advances, several limitations remain in current data-driven resistance spot welding research. Most existing studies still focus on the forward prediction problem, where welding parameters or process signals are mapped to weld quality indicators. In contrast, the inverse problem of directly generating welding schedules according to material-stack characteristics and prescribed weld quality targets has received relatively limited attention. Furthermore, many existing models are developed under specific material systems, welding equipment, and predefined process windows, resulting in uncertain generalization capability when applied to new sheet combinations or different vehicle manufacturing scenarios. Although physical knowledge has increasingly been incorporated into data-driven models, it is generally introduced as auxiliary features rather than explicit constraints within the parameter generation process. Therefore, how to utilize physically meaningful constraints to reduce the ambiguity of feasible welding schedules and achieve reliable parameter generation remains an important challenge for intelligent resistance spot welding. However, purely data-driven models face a critical non-uniqueness problem. For a given stack-up combination and target nugget size, multiple feasible welding schedules may exist, such as a high-current/short-time schedule or a low-current/long-time schedule. A model trained solely on sample statistics may learn an averaged or inconsistent solution, leading to poor accuracy or physical implausibility under distribution shifts, especially across vehicle models.

To address this fundamental challenge, this work proposes a physics-constrained ensemble-learning framework centered on heating intensity, an interpretable intermediate variable that quantifies the temporal concentration of heat input during welding. A multi-loss model jointly optimizes parameter-prediction accuracy and heating-intensity consistency, guiding the learner to distinguish among alternative welding schedules and compress the multi-solution space. The resulting model produces more unique, physically consistent parameter combinations and exhibits improved cross-vehicle generalization relative to the purely data-driven baseline. This work is organized as follows: Section 2 details the development of the baseline and the proposed physics-constrained ensemble learning models. Section 3 presents the experimental setup and results, evaluating the model's performance. Section 4 provides a thorough discussion and mechanistic analysis of the heating intensity's role. Finally, the paper concludes with a summary of findings and future work.

2. Dataset and Model Development

2.1 Dataset

The experimental dataset used for model development was compiled from production records provided by NIO. The metal sheets covered low-carbon steels (CR01 and CR04), high-strength steels (DP590 and DP780), and ultra-high-strength steel (PHS1300T). Their coating conditions and thicknesses are summarized in Table 1. A total of 450 unique two- or three-sheet stack-up configurations were formed from these materials; 70% were three-layer stacks and 30% were two-layer stacks. For each configuration, the associated welding parameters were collected. Because the production lines used a two-pulse current schedule, the process was characterized by six variables: electrode force (F_a), preheating time (t_p), preheating current (I_p), cooling time (t_c), welding time (t_w), and welding current (I_w). Their ranges and distributions are presented in Table 2.

Table 1. Metal sheet information

Steel grade	Surface status	Thickness / mm
CR01	Galvanized	0.65/0.7/0.8/1
CR04	Bare	0.7/0.8
420LA	Galvanized	0.8/1.0/1.2
DP590	Galvanized	1/1.2/1.4/1.6/2
DP780	Galvanized	1.2/1.4/1.6/1.8
DP980	Galvanized	1/1.8
PHS1300T	Al-Si coated	1.2/1.4/1.6/1.8

Table 2. Welding schedule and welding parameter ranges

Schematic Diagram	Symbol	Parameter	Range
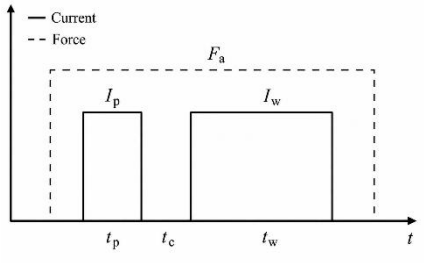	F_a	Electrode force (kN)	2–4.8
	t_p	Preheating time (ms)	50–500
	I_p	Preheating current (kA)	2.5–8
	t_c	Cooling time (ms)	20–100
	t_w	Welding time (ms)	150–800
	I_w	Welding current (kA)	5–13

The 450 unique stack-up configurations originated from two vehicle models: a sedan (Vehicle 1) and a sport utility vehicle (Vehicle 2). Vehicle 1 contained 265 configurations and Vehicle 2 contained 385, with approximately 200 configurations common to both models. Although the common stack-ups had identical sheet information, the welding parameters differed because the production lines and equipment were not the same. Figure 1 compares the parameter distributions for these overlapping configurations. The electrode force, welding current, and welding time differ considerably between the two models, leading to corresponding differences in nugget-diameter distributions. It is therefore unreasonable to expect feasible parameters from sheet-stack information alone. Even for the same stack-up, different schedules can produce different nugget sizes; the model must receive both the stack-up configuration and the target nugget size to generate an appropriate parameter set.

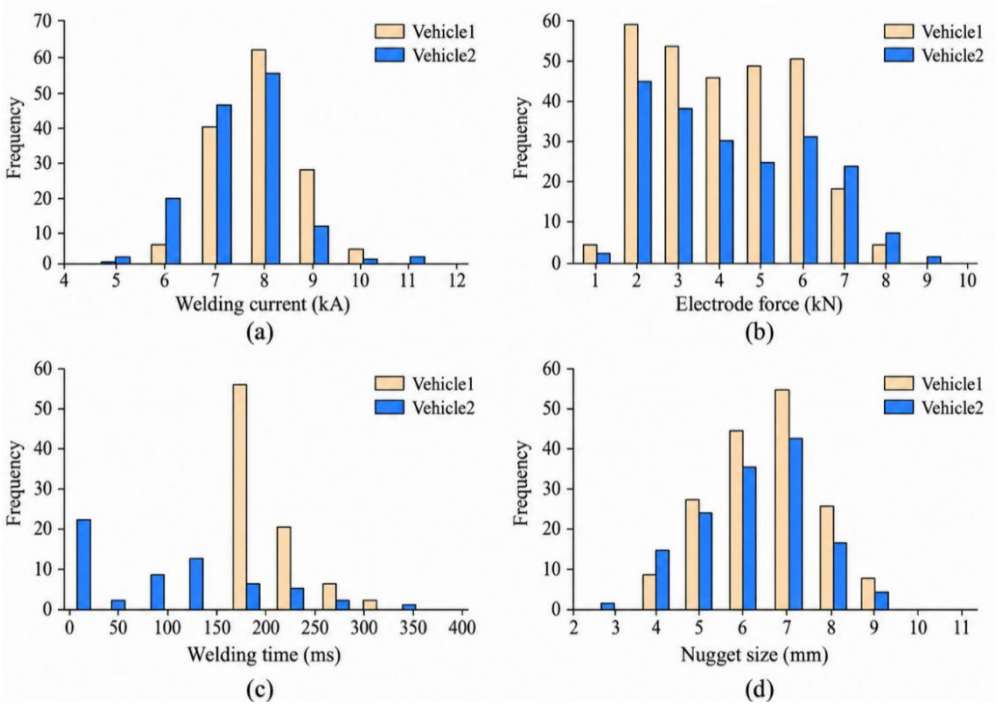

Figure 1. Welding parameters and nugget size distribution involved in two different vehicle models: (a) welding current, (b) electrode force, (c) welding time, and (d) nugget size.

2.2 Baseline Ensemble Learning Model

Figure 2 illustrates the shared ensemble architecture and weighted aggregation strategy used by the baseline and physics-constrained variants. The baseline uses sheet thickness, sheet strength, sheet-stack combination, coating information, and target nugget size as inputs, and predicts six process parameters: electrode force, preheating time, preheating current, cooling time, welding time, and welding current. The physics-constrained variant additionally uses target heating intensity and its corresponding loss term, as detailed in Section 2.3. Input data are normalized before being supplied to heterogeneous base learners, and their outputs are fused through weights determined from five-fold cross-validation. The base learners are Gaussian process regression (GPR), random forest regression (RFR), multilayer perceptron (MLP), support vector regression (SVR), LightGBM, and XGBoost. Their complementary fitting, feature-learning, and robustness characteristics help represent the nonlinear mapping from sheet-stack and quality requirements to welding parameters.

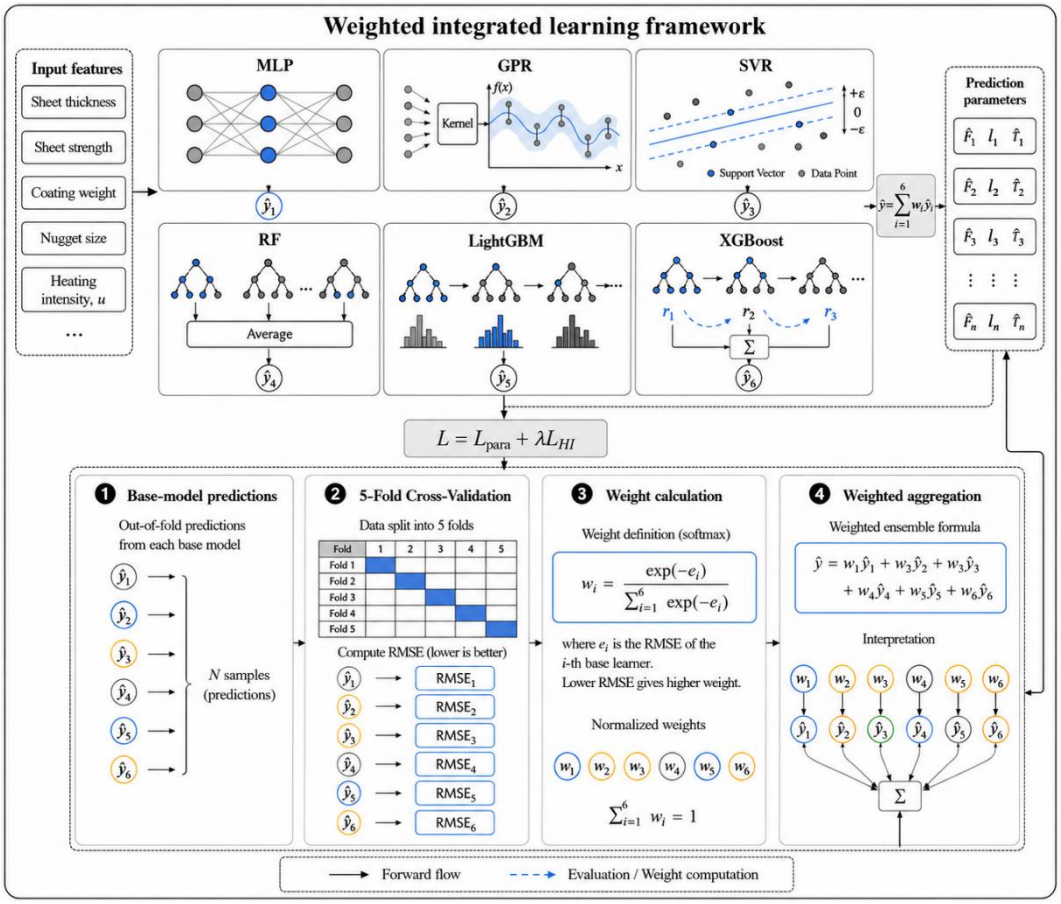

Figure 2. Architecture and weighted aggregation strategy of the ensemble-learning framework

After the individual base learners are trained, their outputs are fused using a weighted ensemble rather than simple averaging. Because the predictive performance of different base learners varies across output parameters, assigning identical weights would weaken the contribution of the better-performing models. Therefore, weights are allocated according to the prediction errors of the base learners so that

models with lower error contribute more to the final ensemble output. Let the prediction of the i-th base learner be denoted by y_i and its corresponding weight by w_i. The final ensemble output is calculated according to (1). It is obtained as the weighted sum of the predictions of all base learners. i.e.,

$$\begin{cases} \hat{y} = \sum_i w_i y_i \\ w_i = \dfrac{\exp(-\varepsilon_i)}{\sum_i \exp(-\varepsilon_i)} \end{cases} \tag{1}$$

where ε_i is taken as the root mean square error (RMSE) between y_i and its corresponding true value y. This strategy makes it possible to exploit the complementary advantages of different models and to improve both the stability and the overall accuracy of the prediction results.

2.3 Physics-Constrained Ensemble Learning Model

Building on the baseline, the physics-constrained ensemble-learning model introduces heating intensity as a constraint on parameter generation. This constraint characterizes the heat-input path and addresses the non-uniqueness of a purely data-driven model. Similar nugget sizes can be produced by different parameter combinations: as illustrated in Figure 3, two schedules with substantially different welding currents and times both yield nugget sizes of approximately 4.12 mm. The final nugget size alone therefore cannot uniquely determine the process parameters. The same sheet stack-up and target nugget size may correspond to multiple schedules with different heat-input paths.

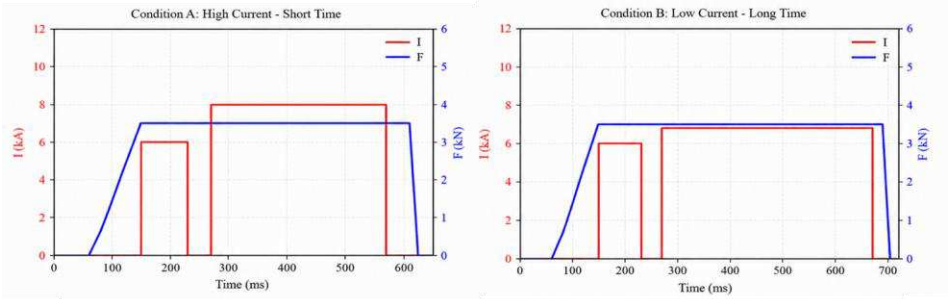

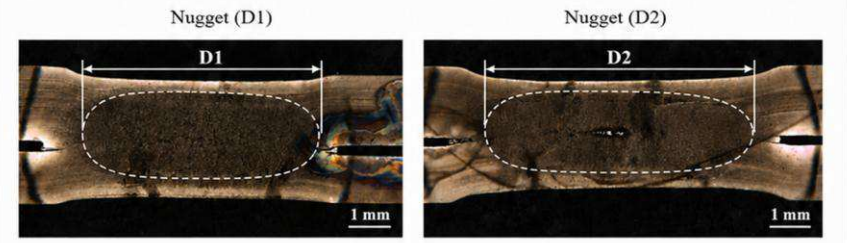

Welding schedule	Electrode force / kN	Preheating current / kA	Preheating time / ms	Cooling time / ms	Welding current / kA	Welding time / ms
Condition A	3.5	6.0	80	40	8.0	300
Condition B	3.5	6.0	80	40	6.8	400

Figure 3. Comparison of similar nugget sizes produced by different welding schedules

Heating intensity (u) is defined by (2), as a derived variable that characterizes the heat input path. It is defined as the ratio of the square of the average welding current ($\overline{I}$) to the total welding time (T):

$$u = \frac{\overline{I}^2}{T} = \frac{t_p I_p^2 + t_w I_w^2}{\left(t_p + t_c + t_w\right)^2} \tag{2}$$

According to (2), a larger value of (u) represents a more concentrated heat-input path associated with a high-current, short-time hard welding schedule, whereas a smaller value represents a gentler heat-input path associated with a low-current, long-time soft welding schedule. By including this variable, the model learns the relationship between the input features and a specified heat-input strategy, thereby resolving the multi-solution problem. Physically, a larger u represents more concentrated heat input, while a smaller u represents gentler heat input. Figure 4 schematically illustrates this distinction.

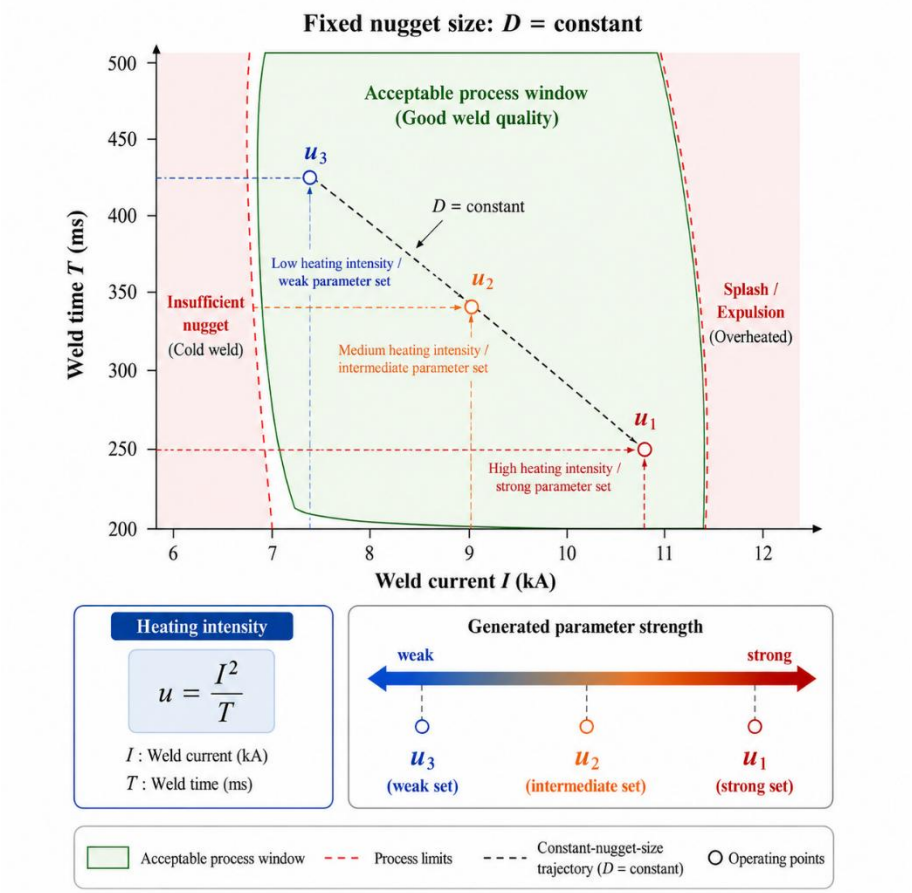

Figure 4. Schematic of heating intensity

To incorporate the heating-intensity constraint into model training, the combined training objective is defined in (3) as a weighted sum of the parameter-prediction loss and the heating-intensity loss.

$$L = L_{para} + \lambda L_{HI} \tag{3}$$

where L_{para} penalizes the deviation between the generated welding parameters and the measured process

parameters; it can combine the individual losses for each output. L_{HI} penalizes the deviation between the heating intensity calculated from the generated parameters and the target heating intensity calculated from the measured parameters. This term guides the model toward parameter sets that follow a specified heat-input path. The coefficient λ balances parameter accuracy against physical consistency. Thus, the multi-loss objective changes the task from fitting parameters alone to fitting parameters while respecting the prescribed heat-input relationship.

3. Experimental Results

3.1 Model Optimization

3.1.1 Optimization of the Baseline Ensemble Learning Model

To ensure a robust comparison, both the baseline and physics-constrained models were optimized. Key hyperparameters for the six base learners were identified using a systematic search, as detailed in Table 3. The goal was to select the configuration that minimized the overall relative error for each base learner, establishing a solid foundation for the ensemble models.

Table 3. Hyperparameter search space of the base learners

Hyperparameter group	GPR: kernel function	MLP: hidden-layer structure	RF: number of trees	SVR: kernel function	LightGBM: number of trees	XGBoost: number of trees
1	RBF	100/50/500	100	RBF	100	100
2	Matern	150/100/1000	200	Linear	500	500
3	Rational Quadratic	200/150/1500	300	Polynomial	1000	1000
4	Hybrid	250/200/2000	400	Sigmoid	1500	1500

Figure 5 shows the results of hyperparameter tuning. Different base learners have different optimal settings. For Gaussian process regression, the rational quadratic kernel works best. It gives lower errors than the RBF, Matérn, and hybrid kernels for most outputs. Therefore, we select it as the final kernel. For the multilayer perceptron, the hidden-layer structure clearly affects performance. The 250/200/2000 layout achieves the lowest overall error, so it is well suited for this welding-parameter prediction task. For random forest, more trees generally lead to better performance. The lowest error occurs at 400 trees. For support vector regression, the polynomial kernel shows better stability and lower error than the RBF, linear, and sigmoid kernels. For the boosting models, LightGBM and XGBoost perform best with 1500 and 100 trees, respectively. This difference suggests that the two models need different levels of complexity for this dataset.

Based on these results, we set each base learner to its best configuration. These optimized models

are then used as building blocks for the ensemble. Tuning each model separately before ensemble construction is important. It prevents poor base-learner settings from hiding the true performance of the ensemble. As a result, the final conclusions become more reliable.

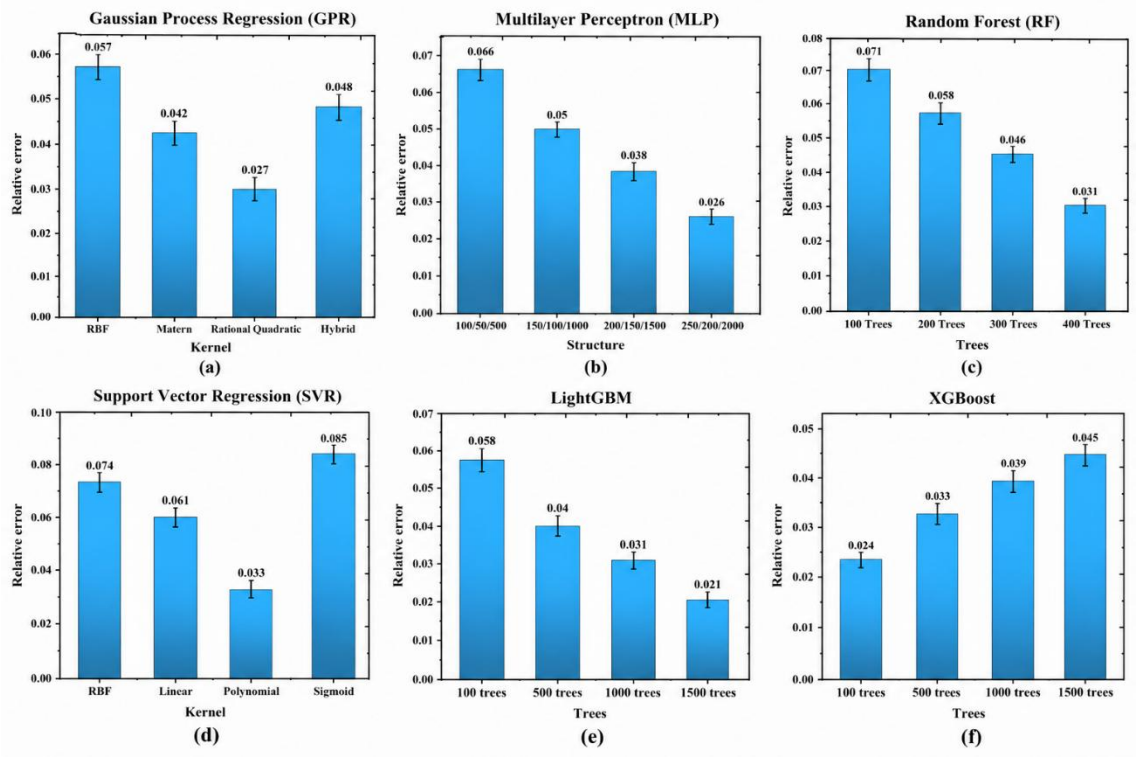

Figure 5. Comparison of hyperparameter optimization results for the base learners: (a) kernel functions of Gaussian process regression (GPR); (b) hidden-layer structures of the multilayer perceptron (MLP); (c) numbers of trees in random forest (RF); (d) kernel functions of support vector regression (SVR); (e) numbers of trees in LightGBM; and (f) numbers of trees in XGBoost.

3.1.2 Optimization of the Physics-Constrained Model

To further improve the accuracy, stability, and cross-vehicle generalization of the physics-constrained model, the fixed loss weighting in the multi-loss framework was replaced with an adaptive strategy. Because the parameter and heating-intensity losses differ in magnitude, convergence rate, and physical meaning, fixed empirical weights can cause one objective to dominate training. Following the uncertainty-based loss-weighting approach proposed by Kendall et al. [33], learnable uncertainty parameters were introduced to balance the two losses. After each loss was normalized by its initial value, the fixed-weight objective in (3) was reformulated as (4):

$$L = \frac{1}{2s_1^2} L_{para} + \frac{1}{2s_2^2} L_{HI} + \log S_1 S_2 \tag{4}$$

In (4), s_1 and s_2 are learnable parameters associated with the uncertainties of the parameter and heating-intensity losses, respectively. The strategy avoids grid search for fixed loss weights and

dynamically balances the gradient contributions of the two objectives in the shared feature space. This balance is important because an overemphasis on numerical fitting can suppress the physical constraint and weaken generalization or parameter uniqueness. The two losses represent parameter-fitting and physical-consistency objectives, respectively. Adaptive weighting therefore allows the model to learn physically consistent relationships while maintaining high prediction accuracy, providing a robust basis for cross-vehicle and multi-stack RSW parameter generation.

3.2 Model Evaluation

The performance of the models was rigorously evaluated under two key scenarios: same-vehicle and cross-vehicle parameter generation.

3.2.1 Same-Vehicle Parameter Generation

In the same-vehicle test, both models were trained and evaluated using data from the same vehicle model. Figure 6 shows that the optimized baseline already achieves high prediction accuracy, while the physics-constrained model provides consistent improvements across all six output parameters. The largest gain is observed for preheating time, increasing from 95.3% to 97.5%. The mean accuracy gain across the six output parameters is approximately 1.35 percentage points. These results indicate that the heating-intensity constraint provides additional improvement even when the training and test data originate from the same vehicle distribution.

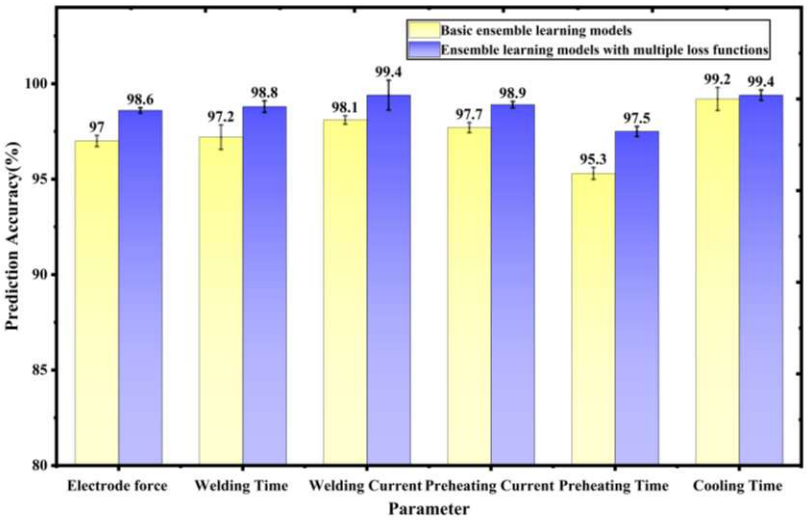

Figure 6. Comparison of parameter-generation performance under same-vehicle conditions

3.2.2 Cross-Vehicle Parameter Generation Test

The cross-vehicle test provides the critical evaluation of generalization. Models trained using Vehicle 1 were tested using Vehicle 2, and vice versa. As shown in Figure 7, the baseline ensemble-learning model exhibits a clear performance degradation under cross-vehicle transfer, particularly for

preheating-current prediction, where the accuracies decrease to 64.3% and 71.1% in the two transfer directions. These results reveal the limited adaptability of the purely data-driven baseline to shifted vehicle-specific data distributions.

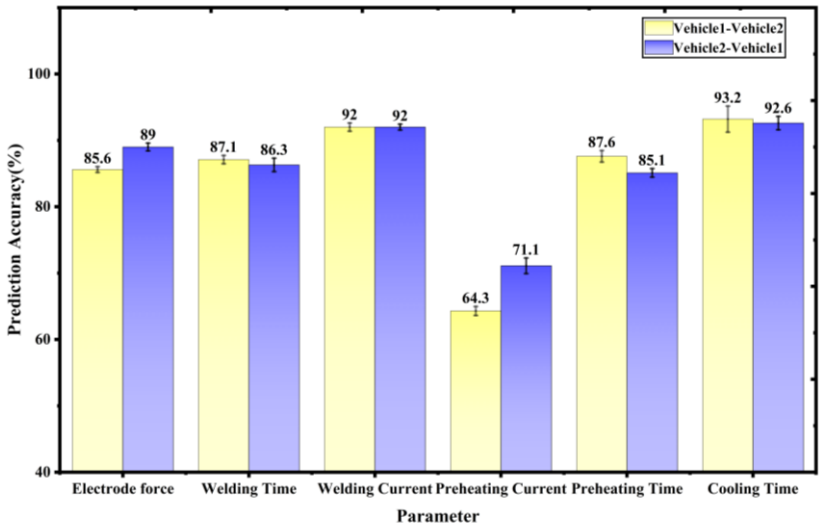

Figure 7. Cross-vehicle parameter-generation results of the baseline ensemble learning model

In contrast, the physics-constrained model maintains substantially stronger performance in both transfer directions. Figure 8 shows accuracies ranging from 79.9% to 95.8% across the six predicted parameters, with welding-current accuracy remaining above 95% in both directions. Compared with the baseline results in Figure 7, the physics-constrained model obtains a gain up to 15.6% (from 64.3% to 79.9%), and improves the overall mean cross-vehicle prediction accuracy from approximately 85.5% to 90.0%. The reduced gap between same-vehicle and cross-vehicle tests indicates that the heating-intensity constraint encourages the model to learn process relationships that transfer across vehicle datasets rather than vehicle-specific statistical patterns.

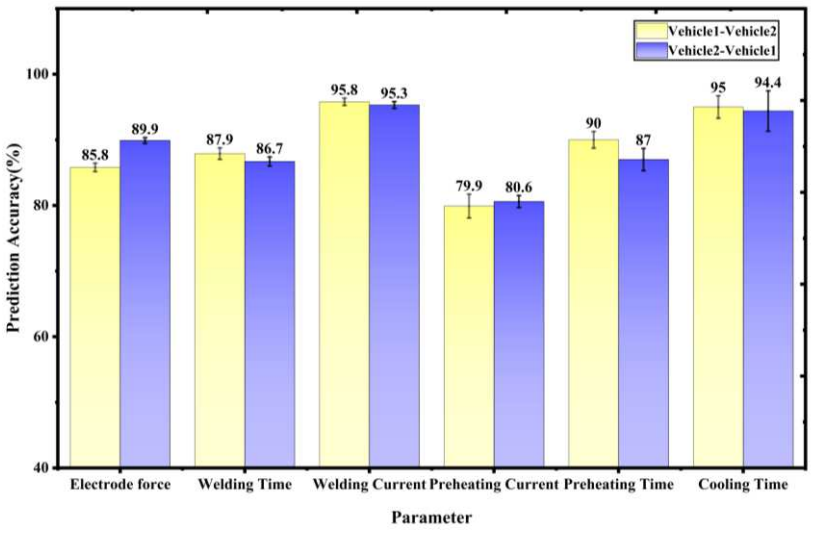

Figure 8. Cross-vehicle parameter-generation results of the multi-loss ensemble learning model

4. Discussion and Analysis

The experimental results clearly demonstrate the superiority of the physics-constrained model, particularly in cross-vehicle scenarios. This section delves into the mechanistic reasons for this improvement, focusing on the role of the heating intensity constraint.

4.1 Constraining the Solution Space via Heating Intensity

The primary challenge addressed by the proposed framework is the non-uniqueness of parameter solutions. To verify the constraining effect of heating intensity, a sensitivity analysis was performed using a representative two-sheet stack-up consisting of 1.0 mm galvanized DP590 and 1.2 mm galvanized DP780. The sheet stack-up, target nugget size, and electrode force were held constant while the target heating intensity was increased incrementally.

As shown in Table 4, increasing the target heating intensity from 0.25 to 0.40 led to a systematic decrease in the predicted welding time from 300 to 232 ms, accompanied by an increase in the predicted welding current from 8.9 to 9.4 kA. To verify whether these generated schedules could still achieve the prescribed weld quality, four welds were produced using the corresponding parameter sets. The measured nugget diameters were 5.02, 5.01, 5.09, and 4.96 mm, respectively, remaining close to the target nugget diameter of approximately 5.0 mm. These results demonstrate that varying the heating intensity changes the current–time combination and hence the heat-input path, while preserving the required nugget size.

Without the heating intensity constraint, the model is faced with a multi-solution problem where multiple valid parameter combinations can produce the same target nugget size. A purely data-driven model might learn an average representation of these solutions, leading to poor performance when a specific solution path is required. By introducing heating intensity as a constraint, we add a new dimension of information that explicitly encodes the heat input strategy. This forces the model to map the input features to a specific point in the solution space, effectively compressing the multi-solution space into a uniquely defined feasible region. This is the fundamental reason why the model generates parameters with enhanced uniqueness and physical consistency.

Table 4. Test settings for the heating-intensity sensitivity analysis

Case	Heating intensity	Predicted welding time / ms	Predicted welding current / kA	Measured nugget size / mm
1	0.25	300	8.9	5.02
2	0.30	282	9.2	5.01
3	0.35	260	9.3	5.09
4	0.40	232	9.4	4.96

4.2 Heating Intensity as a Mechanism for Controllable Parameter Generation

Beyond improving accuracy and uniqueness, the heating intensity constraint provides a powerful mechanism for controllable generation. By treating heating intensity as an adjustable input parameter, the model can be used to purposefully generate hard or soft welding schedules. This is a significant engineering advantage. For example, in a high-volume production environment, a "hard" schedule (high current, short time) might be preferred to minimize cycle time. Conversely, for materials prone to expulsion, a "soft" schedule (low current, long time) might be more appropriate. The ability to generate parameters based on a user-defined heating intensity enables process engineers to tailor the welding schedule to specific production constraints, making the model a practical and flexible tool for process planning.

Figure 9 compares the generated current-time pairs for three representative sheet combinations as the target heating intensity is swept from 0.1 to 0.9. Despite stack-dependent shifts in the feasible current-time region, all three combinations exhibit the same monotonic progression: low u yields low-current/long-time soft schedules, intermediate u produces medium schedules, and high u yields high-current/short-time hard schedules. The consistent trajectories demonstrate that u provides a transferable control variable, whereas the absolute current and time remain material-stack dependent. This behavior gives process engineers a practical way to select schedules according to production priorities: softer schedules can help limit expulsion or indentation, while harder schedules can reduce cycle time. By adjusting the target heating intensity, the framework automatically derives a corresponding current-time combination in a physically interpretable manner.

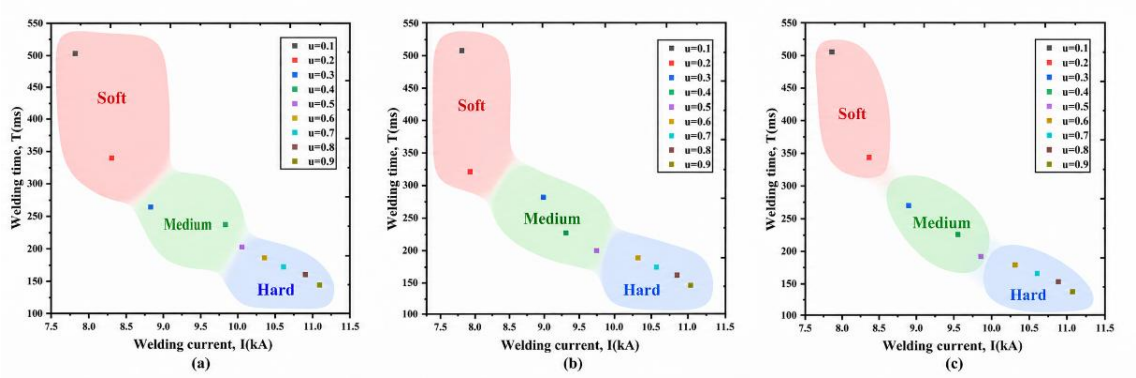

Figure 9. Distribution of parameter combinations under different heating intensities: (a) sheet combination A; (b) sheet combination B; and (c) sheet combination C.

4.3 The Role of Physics in Cross-Vehicle Generalization

To assess the contribution of the heating-intensity constraint, an ablation study was conducted by removing the heating-intensity loss term (L_{HI}, also *Loss2*) from the full model while retaining the parameter-fitting loss (L_{para}, also *Loss1*). All other components, including the base-learner structure, data-

splitting strategy, training procedure, and ensemble scheme, were unchanged. As shown in Figure 10, under same-vehicle conditions the full model improves parameter-wise prediction accuracy by 0.0–2.3 percentage points relative to the parameter-loss-only variant, with the largest gain observed for preheating time. Although the ablated model retains high numerical accuracy, the consistent gains from the combined-loss model show that Loss2 helps guide learning toward physically consistent parameter combinations.

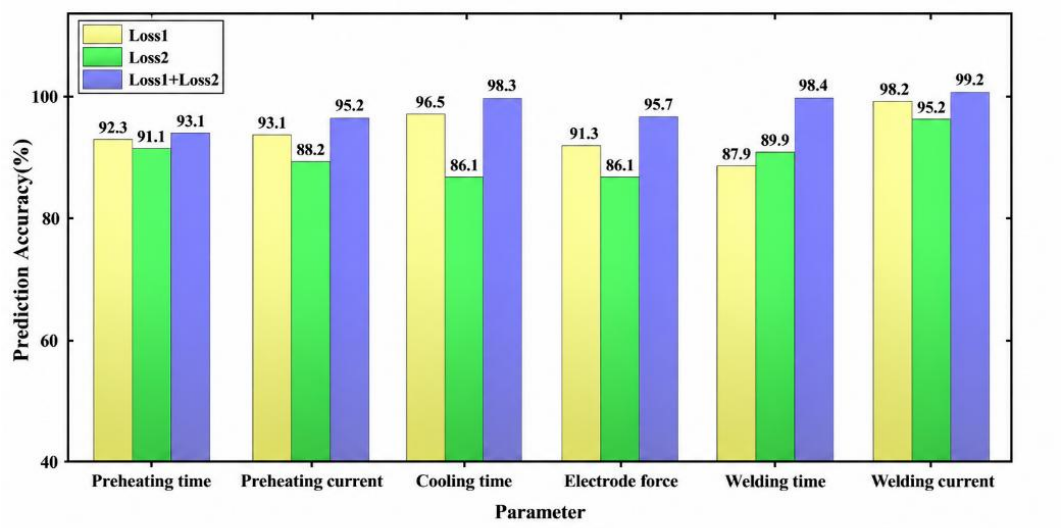

Loss	Preheating time	Preheating current	Cooling time	Electrode force	Welding time	Welding current
Loss1	92.30%	93.10%	96.50%	91.30%	87.90%	98.20%
Loss2	91.10%	88.20%	86.10%	86.10%	89.90%	95.20%
Loss1+Loss2	93.10%	95.20%	98.30%	95.70%	98.40%	99.20%

Figure 10. Prediction accuracy of the ablation study under same-vehicle conditions

A major benefit of the heating-intensity constraint is its contribution to cross-vehicle generalization. Data from different vehicle models originate from production environments with distinct equipment, preferred schedules, and cycle-time requirements. A purely data-driven model can absorb these environment-specific correlations and incur errors after transfer. The physics-constrained model is instead required to generate parameters that satisfy the same physically meaningful heat-input relationship. Figure 11 makes the difference clear: removing Loss2 reduces accuracy by 0.1–15.6 percentage points across the two transfer directions, with the largest loss occurring for preheating-current prediction in the Vehicle 2-to-Vehicle 1 transfer. These larger out-of-distribution penalties show that the physical constraint contributes most when the model is transferred beyond its training distribution.

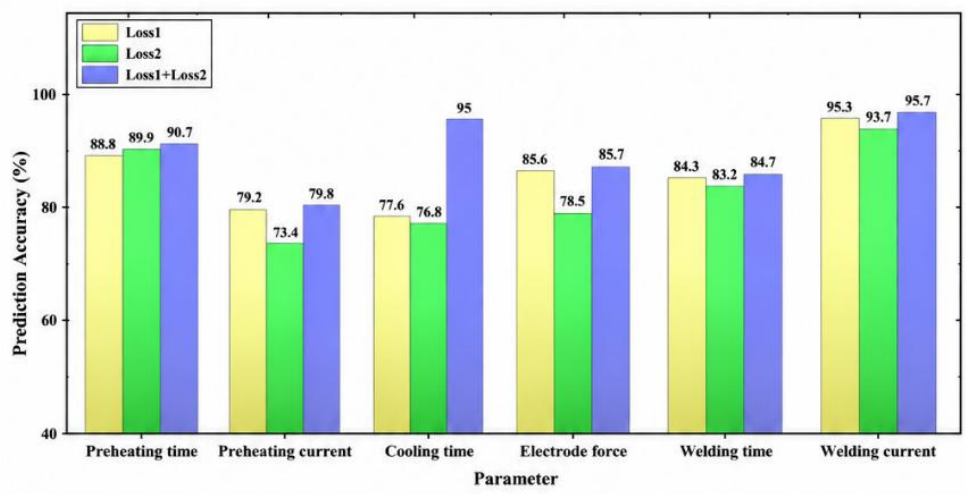

Loss	Preheating time	Preheating current	Cooling time	Electrode force	Welding time	Welding current
Loss1	88.80%	79.20%	77.60%	85.60%	84.30%	95.30%
Loss2	89.90%	73.40%	76.80%	78.50%	83.20%	93.70%
Loss1+Loss2	90.70%	79.80%	95.00%	85.70%	84.70%	95.70%

(a)

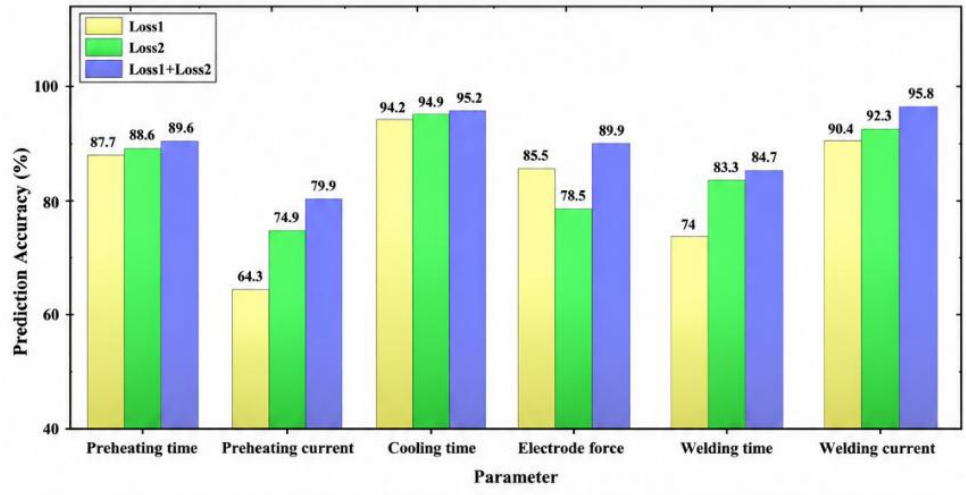

Loss	Preheating time	Preheating current	Cooling time	Electrode force	Welding time	Welding current
Loss1	87.70%	64.30%	94.20%	85.50%	74.00%	90.40%
Loss2	88.60%	74.90%	94.90%	78.50%	83.30%	92.30%
Loss1+Loss2	89.60%	79.90%	95.20%	89.90%	84.70%	95.80%

(b)

Figure 11. Prediction accuracy of the ablation study under cross-vehicle transfer conditions: (a) training on Vehicle 1 and testing on Vehicle 2; (b) training on Vehicle 2 and testing on Vehicle 1.

5. Conclusions

This paper presented a physics-constrained ensemble learning framework for the rapid and reliable design of resistance spot welding parameters. The central innovation is the integration of the heating intensity constraint into a multi-loss ensemble learning model, moving beyond purely data-driven regression to a mechanism-data fusion approach. The key findings and conclusions are summarized as

follows:

(1) The proposed framework outperforms the baseline ensemble-learning model, particularly under cross-vehicle transfer. By embedding a physical constraint, the model learns more transferable process relationships and achieves a cross-vehicle accuracy gain up to 15.6% among the six predicted parameters.
(2) The introduction of heating intensity as an explicit constraint effectively compresses the multi-solution space inherent in RSW parameter design. The sensitivity analysis confirmed that the model generates unique and deterministic parameter sets for a given target heating intensity, ensuring that the predicted parameters are not only numerically accurate but also physically consistent and interpretable.
(3) The framework enables the engineering control of the welding schedule. By adjusting the target heating intensity, the model can be directed to generate "hard" (high current/short time) or "soft" (low current/long time) parameters, offering practical flexibility for optimizing cycle times or mitigating weld defects.

Future work will focus on extending the framework to accommodate more complex welding waveforms, such as multi-pulse schedules with varying current amplitudes, and to integrate additional physical constraints, such as electrode force and material-specific thermal properties. The development of a real-time parameter recommendation system is also a key objective for future industrial deployment.

Author contribution

Yu-Jun Xia: conceptualization, methodology, validation, formal analysis, investigation, writing—original draft, and writing—review and editing. YunFan Zhou: investigation, data curation, and writing—review and editing. YouRong Zhang: methodology, formal analysis, and writing—review and editing. JianNan Zhang: methodology, validation, and visualization. YongQuan Jia: project administration. YongBing Li: resources, funding acquisition, and supervision.

Declarations

The authors declare no competing interests.

Acknowledgments

The authors gratefully acknowledge financial support from the National Natural Science Foundation of China (Grant No. 52575415), the Fundamental and Interdisciplinary Disciplines Breakthrough Plan of the Ministry of Education of China, the State Key Laboratory of Mechanical System and Vibration (Grant No. MSVZD202603), and NIO University Program (NIO UP).

References

[1] Yu F, Tang H, Zhu F, Geng P, Wan H, Xia Y J, Wang X, Ma Y, Li Y. Critical role of feed depth in governing rivet/SUS interfacial behavior of friction stir riveted CFRP/SUS joints [J]. Journal of Manufacturing Processes, 2026, 157: 1182 – 1192.

[2] Zhang Y, Li J, Huang H, Li Y, Morisada Y, Fujii H, Liu H. Cooperative deformation mechanism and its role on defect elimination in pressure-controlled Joule-heat forge welding of Ti – 6Al – 4V/SUS316L dissimilar metals [J]. Journal of Materials Research and Technology, 2026, 42: 1 – 14.

[3] Huang H, Wang Y, Chen J, Li Y, Feng Z. On the roles of welding residual stresses in determination of fracture toughness in austenitic stainless steel SUS 304 pipeline girth welds [J]. Engineering Fracture Mechanics, 2026, 334: 111871.

[4] Wan H, Ma Y, Geng P, Wang H, Min J, Li Y. Laser-induced multiscale surface structuring of titanium bipolar plates for interface strengthening in adhesive sealing [J]. Journal of Materials Science & Technology, 2027, 281: 140 – 150.

[5] Xia Y J, Zhang Z D, Xia Z X, Zhu S L. A precision analogue integrator system for heavy current measurement in MFDC resistance spot welding [J]. Measurement Science and Technology, 2016, 27(2): 025104.

[6] Karim M A, Park Y D. A review on welding of dissimilar metals in car body manufacturing [J]. Journal of Welding and Joining, 2020, 38(1): 8 – 23.

[7] Stavropoulos P, Sabatakakis K. Quality assurance in resistance spot welding: state of practice, state of the art, and prospects [J]. Metals, 2024, 14(2): 185.

[8] Martín Ó, De Tiedra P. Advances in the control and improvement of quality in the resistance spot welding process [J]. Metals, 2022, 12(11): 1810.

[9] Aslanlar S. The effect of nucleus size on mechanical properties in electrical resistance spot welding of sheets used in automotive industry [J]. Materials & Design, 2006, 27(2): 125 – 131.

[10] Aslanlar S, Ogur A, Ozsarac U, Ilhan E, Demir Z. Effect of welding current on mechanical properties of galvanized chromided steel sheets in electrical resistance spot welding [J]. Materials & Design, 2007, 28(1): 2 – 7.

[11] Hayat F, Sevim I. The effect of welding parameters on fracture toughness of resistance spot-welded galvanized DP600 automotive steel sheets [J]. The International Journal of Advanced Manufacturing Technology, 2012, 58(9 – 12): 1043 – 1050.

[12] Geng P H, Xia Y J, Dong Z Q, Men B X, Pan B, Shao C H, Li Y B, Li J J. Machine learning

applications in welding processes: Progresses and opportunities [J]. International Journal of Machine Tools and Manufacture, 2025, 213: 104344.

[13] Ma C, Chen D L, Bhole S D, Boudreau G, Lee A, Biro E. Microstructure and fracture characteristics of spot-welded DP600 steel [J]. Materials Science and Engineering: A, 2008, 485(1–2): 334–346.

[14] Khan M I, Kuntz M L, Biro E, Zhou Y. Microstructure and mechanical properties of resistance spot welded advanced high strength steels [J]. Materials Transactions, 2008, 49(7): 1629–1637.

[15] Kim T, Park H, Rhee S. Optimization of welding parameters for resistance spot welding of TRIP steel with response surface methodology [J]. International Journal of Production Research, 2005, 43(21): 4643–4657.

[16] Lin H L, Chou C P, Tseng C H. Optimization of resistance spot welding process using Taguchi method and a neural network [J]. Experimental Techniques, 2007, 31(5): 30–36.

[17] Cho Y, Rhee S. Quality estimation of resistance spot welding by using pattern recognition with neural networks [J]. IEEE Transactions on Instrumentation and Measurement, 2004, 53(2): 330–334.

[18] El Ouafi A, Bélanger R, Méthot J F. Artificial neural network-based resistance spot welding quality assessment system [J]. Metallurgical Research & Technology, 2011, 108(6): 343–355.

[19] Yu J. Quality estimation of resistance spot weld based on logistic regression analysis of welding power signal [J]. International Journal of Precision Engineering and Manufacturing, 2015, 16(13): 2655–2663.

[20] Xia Y J, Lv T L, Ghassemi-Armaki H, Li Y B, Carlson B E. Quantitative interpretation of dynamic resistance signal in resistance spot welding [J]. Welding Journal, 2023, 102(4): 69s–87s.

[21] Xing B, Xiao Y, Qin Q H, Cui H. Quality assessment of resistance spot welding process based on dynamic resistance signal and random forest [J]. The International Journal of Advanced Manufacturing Technology, 2018, 94: 327–339.

[22] Zamanzad Gavidel S, Lu S, Rickli J L. Performance analysis and comparison of machine learning algorithms for predicting nugget width of resistance spot welding joints [J]. The International Journal of Advanced Manufacturing Technology, 2019, 105(9): 3779–3796.

[23] Zhou B, Pychynski T, Reischl M, Kharlamov E, Mikut R. Machine learning with domain knowledge for predictive quality monitoring in resistance spot welding [J]. Journal of Intelligent Manufacturing, 2022, 33(4): 1139–1163.

[24] Dai W, Li D, Zheng Y, Wang D, Tang D, Wang H, Peng Y. Online quality inspection of resistance spot welding for automotive production lines [J]. Journal of Manufacturing Systems, 2022, 63: 354–

369.

[25] Xia Y J, Li Z R, Wang W J, Yang T H, Pi G, Li Y B. Influence mechanism of initial gap disturbance on the resistance spot welding process [J]. Automotive Innovation, 2024, 7(2): 360–372.

[26] He Y, Yang K, Wang X, Huang H, Chen J. Quality prediction and parameter optimisation of resistance spot welding using machine learning [J]. Applied Sciences, 2022, 12(19): 9625.

[27] Deng X, You W, Xu H. Prediction of resistance spot welding parameters by Bayes-XGBoost and particle swarm optimization [J]. Journal of Electronics & Information Technology, 2021, 43(4): 1042–1049.

[28] Bayır M, Yücel E, Kaya T, Yıldırım N. Spot welding parameter tuning for weld defect prevention in automotive production lines: an ML-based approach [J]. Information, 2023, 14(1): 50.

[29] York E, Zhao X, Ghessemi-Armaki H, Carlson B, Wang P. Transfer learning-enhanced transformer for virtual process sensing in resistance spot welding [J]. Manufacturing Letters, 2025, 45: 13–16.

[30] Yang K, Li C, Beck R, Hein D, Meschut G. A physics-guided hybrid framework for online pre-expulsion prediction in resistance spot welding [J]. Journal of Manufacturing Processes, 2026, 174: 135–153.

[31] Xia Y J, Song Q, Yi B, Lyu T, Sun Z, Li Y. Improving out-of-distribution generalization for online weld expulsion inspection using physics-informed neural networks [J]. Welding in the World, 2025, 69(5): 1309–1322.

[32] Lv T L, Xia Y J, Murugan S P, Okigami F, Ghassemi-Armaki H, Carlson B E, Li Y. Multi-physical process simulation of resistance spot welding available for synthetic data generation [J]. Journal of Manufacturing Processes, 2025, 141: 709–724.

[33] Kendall A, Gal Y, Cipolla R. Multi-task learning using uncertainty to weigh losses for scene geometry and semantics. Proceedings of the IEEE Conference on Computer Vision and Pattern Recognition, 2018: 7482–7491.